Performance Comparison of Handover Mechanisms for LEO Networks in S and Ka-bands

Xhelja Kodheli*, Muhammad Sohaib J. Solaija*†, and Hüseyin Arslan*

*Department of Electrical and Electronics Engineering, Istanbul Medipol University, Istanbul, 34810 Turkey
*Institute of Defence Technologies, Gebze Technical University, Gebze, Kocaeli, 41400 Turkey
Email: xhelja.kodheli@std.medipol.edu.tr, solaija@ieee.org, huseyinarslan@medipol.edu.tr

2024 IEEE Wireless Communications and Networking Conference (WCNC) | 979-8-3503-0358-2/24/$31.00 ©2024 IEEE | DOI: 10.1109/WCNC57260.2024.10570666

***Abstract*—Low-Earth orbit (LEO) non-terrestrial networks (NTNs) have become increasingly popular due to their ability to provide high-bandwidth communication in otherwise unserved regions. However, this comes at the cost of high satellite mobility, necessitating efficient handover (HO) strategies. Till now the focus has been on the S-band, however Ka-band is expected to be deployed for high-bandwidth applications necessitating HO studies for higher frequency bands. To address this, we evaluate the performance of the conventional received power-based HO, as well as alternatives such as elevation angle and distance-based triggers for Ka-band LEO networks, and compare them with S-band frequencies. Moreover, a dynamic threshold approach is also evaluated in terms of the number of HOs, unnecessary handovers (UHOs), radio link failures (RLFs), and distributions of downlink carrier-to-noise-plus-interference ratio (CNIR) and mean time-of-stay of a user in a cell. The obtained results indicate the efficacy of power-based mechanisms for the S-band while showing that the alternative methods provide a much better balance at the Ka-band in terms of the overhead and the overall communication link quality.**

***Index Terms*—5G, handover (HO), Ka-band, low-Earth orbit (LEO), non-terrestrial network (NTN), radio link failure (RLF), satellite, S-band, very-small-aperture terminal (VSAT).**

I. Introduction

Wireless communication has become an imperative part of our daily lives with the increasing dependence on it for applications such as education, finance, healthcare, public safety, transportation, etc. This requires ubiquitous connectivity which necessitates increasingly heterogeneous network deployments including non-terrestrial networks (NTNs). Compared to other satellite systems such as geostationary Earth orbit (GEO) or medium Earth orbit (MEO), low Earth orbit (LEO) satellites provide lower latency and higher capacity. Due to their smaller footprints and more frequent reuse of the spectrum, these satellites can be used in constellations to provide coverage in remote areas. However, LEO-based systems face several challenges such as limited coverage, short visibility time, high Doppler shift, interference, etc., due to their high mobility.

Given the short visibility time of LEO satellites, proper handover management is essential to ensure the continuity of communication and to avoid service disruptions that can cause delays or data loss. While the conventional mechanisms rely on received signal strength (RSS) measurements to trigger handovers (HOs), this approach is challenging in NTNs due to the significantly low RSS variation (limited to $4-5$ dB between cell center and edges) compared to the terrestrial networks, necessitating the need for other alternatives. In line with this, the work in [1] examines the standard handover algorithm in LEO-based NTNs and compares the performance to 3rd Generation Partnership Project (3GPP) terrestrial scenarios through system-level simulations. The study finds that handover failures (HOFs) and radio link failures (RLFs) are significantly more prevalent in NTNs. In [2], traditional RSS measurement-based HO triggering mechanisms are compared to alternative methods such as distance, elevation angle, and timer-based methods in terms of HO occurrences and RLFs. A location-based HO method is proposed in [3] which eliminates HOFs and unnecessary handovers (UHOs) while extending the service time. Conditional handover (CHO) mechanism is investigated in [4], where it is determined to reduce RLFs and HOFs while increasing UHOs. A further optimization of CHO is given in [5] aimed at enhancing the time-of-stay and reducing HOs. A solution for intra-satellite mobility utilizing predictable satellite movement and antenna gain is given in [6], which eliminates failures, increases time-of-stay in a cell, and improves downlink signal-to-interference-plus-noise ratio (SINR). All of these works, however, are limited to the HO performance in S-band.

While 3GPP Release-17 focuses on frequencies < 10 GHz, higher frequencies (Ka-band) are expected to be part of Release-18 standardization activities. Since the higher frequencies of Ka-band allow for greater bandwidth and capacity compared to lower frequency bands such as S-band while affording lighter and smaller antennas, they are well-suited for high-speed applications such as broadband internet access, video and multimedia streaming, as well as satellite-based navigation and positioning systems, satellite-to-satellite communications and inter-satellite links, and other remote sensing applications. However, the Ka-band also experiences more atmospheric attenuation and is susceptible to interference from water vapor and rain, which affect the signal quality (and range of communication). While higher frequency bands have been studied in the NTN context, these studies are limited to achievable data rates/capacity for millimeter wave (mmWave) band operation [7] and deep reinforcement learning-based HO mechanism in Ku-band [8]. Accordingly, in this work, we try to plug this gap in the literature by:

979-8-3503-0358-2/24/$31.00 ©2024 IEEE

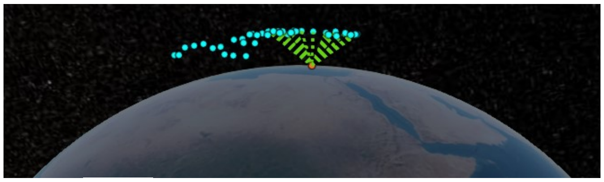

Fig. 1. Illustration of the considered system using Matlab®'s Satellite toolbox. Red circle represents a VSAT/handheld user, blue circles are the Starlink satellites in the vicinity, and green lines represent the active links (between the user and satellites with elevation angle $\theta > 30°$.).

- As opposed to our previous work [2] where only S-band is considered, here we compare the HO performance for both S and Ka-bands, showing that the difference in propagation characteristics indeed leads to different quality of service (QoS) capability.
- Dynamic threshold mechanism is adapted depending on the trajectory of the satellite which minimizes undesirable inter-satellite handovers and reduces the signaling overhead.
- To provide further insights, the alternative HO mechanisms are evaluated in terms of a number of HOs, UHOs, mean time-of-stay (MToS), RLFs and carrier-to-noise-plus-interference ratio (CNIR).

The rest of this paper is organized as follows. The system model is presented in Section II. Section III describes the different HO triggering mechanisms. The performance metrics are presented in Section IV. Section V discusses the results while Section VI presents our concluding remarks.

II. System Model

A. System Architecture

For S and Ka-band, the deployment scenarios "D3" and "D4" are considered, respectively, which refer to carrier frequencies of 2 and 20 GHz [9]. Downlink transmission from satellites to handheld devices (S-band) and VSATs (Ka-band) in an outdoor urban environment within a coverage region of ≈ 20 km[1] is considered using full frequency reuse. To increase practicality, we have used orbital information of the Starlink constellation via its two-line element (TLE) [11] set. Only the satellites with elevation angle $\theta > 30°$ are considered because for smaller elevation angles the received power is very low and the user-satellite link quality is poor [10]. These satellites are determined using MATLAB Aerospace Toolbox. This is illustrated in Fig. 1, where the red and blue circles represent a user and different LEO satellites for a single snapshot. Here the green dashed lines represent the satellites that fulfil the elevation angle criteria at that specific instance.

B. Pathloss

Pathloss consists of basic pathloss, attenuation due to rain and clouds as well as atmospheric absorption, ionospheric and tropospheric scintillation, and the building entry losses [9]. This can be represented by

$$\mathrm{PL} = \mathrm{PL_b} + \mathrm{PL_g} + \mathrm{PL_s} + \mathrm{PL_e}, \quad (1)$$

where $\mathrm{PL_b}$ is the basic pathloss, $\mathrm{PL_g}$ combines the rain, cloud, and atmospheric losses. For frequencies below 6 GHz, the attenuation due to atmospheric gases is considered negligible, hence it is ignored for the S-band. $\mathrm{PL_s}$ represents the losses due to scintillation, and $\mathrm{PL_e}$ denotes the loss in received power due to indoor penetration. However, since D3/D4 deployments only consider outdoor users, $\mathrm{PL_e}$ is taken as zero in this work. The basic pathloss $\mathrm{PL_b}$ is itself defined as

$$\mathrm{PL_b} = \mathrm{PL_{FS}} + \mathrm{SF} + \mathrm{CL}, \quad (2)$$

where $\mathrm{PL_{FS}}$ is the free space path loss (FSPL), SF represents shadow fading and CL is the clutter loss. FSPL is the distance and frequency-dependent loss (in dB) characterized by

$$\mathrm{FSPL} = 32.45 + 20\log_{10}(\mathrm{f_c}) + 20\log_{10}(\mathrm{d}), \quad (3)$$

where $\mathrm{f_c}$ is the carrier frequency in GHz and d represents the 3-D distance (in meters) between the transmitter and receiver. Shadow fading and clutter loss combine to represent the losses in received power due to the various objects in the environment including buildings, trees, foliage, etc. The values of σ_{SF} and CL are provided by 3GPP [9] and reproduced in Table I as a function of the elevation angle θ.

Referring back to (1), $\mathrm{PL_g}$ term for Ka-band combines all the atmospheric losses and is computed by the step-by-step procedure (and parameters) provided in [12] for slant paths. Ionospheric scintillation is only considered for low frequencies below 6 GHz and evaluated as discussed in [9]. While ionospheric scintillation can be ignored in Ka-band, these frequencies are still affected by tropospheric scintillation, which is modeled by following the procedure in [13].

Then the sum of line-of-sight (LoS) and non-line-of-sight (NLoS) components gives the total pathloss expressed by the equation below [14]:

$$\mathrm{PL_{tot}} = \mathrm{Pr_{LoS}}(\theta) * \mathrm{PL_{LoS}} + (1 - \mathrm{Pr_{LoS}}(\theta)) * \mathrm{PL_{NLoS}}, \quad (4)$$

where $\mathrm{Pr_{LoS}}(\theta)$ and $1 - \mathrm{Pr_{LoS}}(\theta)$ are the LoS and NLoS probability for elevation angle θ, respectively, $\mathrm{PL_{LoS}}$ is the LoS pathloss and $\mathrm{PL_{NLoS}}$ is the NLoS pathloss. The LoS probabilities, as a function of θ, are provided in Table I.

III. Handover Methods

A. Conventional Received Power-Based Handover

Measurement-based HOs such as the ones relying on A3 events are commonly used in today's terrestrial networks. Specifically, in an A3 event, the received power from a target satellite needs to be greater than the received power from the active/serving satellite by a certain offset amount for a specified time period, referred to as time-to-trigger (TTT), before the HO is triggered. This condition is represented as:

$$\mathrm{P_t} > \mathrm{P_s} + \mathrm{P_{off}}, \quad (5)$$

[1]This is in line with the beam diameter specified in [10]. The same cell size is assumed for S-band to get a fair comparison.

TABLE I
PATHLOSS PARAMETERS FOR NTNS IN URBAN SCENARIO [9]

Elevation (θ)	Shadow Fading		Clutter Losses		LoS Probability
	LoS	NLoS	S-band	Ka-band	
10°	4	6	34.3	44.3	24.6%
20°	4	6	30.9	39.9	38.6%
30°	4	6	29.0	37.5	49.3%
40°	4	6	27.7	35.8	61.3%
50°	4	6	26.8	34.6	72.6%
60°	4	6	26.2	33.8	80.5%
70°	4	6	25.8	33.3	91.9%
80°	4	6	25.5	33.0	96.8%
90°	4	6	25.5	32.9	99.2%

where P_t and P_s are the received power from the target and serving satellites, respectively, and P_{off} is the power offset margin. The received power, P_R, for any satellite is given by

$$P_R = EIRP + G_a - PL_{tot} \quad (6)$$

where EIRP is equivalent isotropically radiated power, G_a is the receiver antenna gain and PL_{tot} is the total pathloss calculated in the previous section. The initial association in this approach is done based on the maximum received power, i.e., each user is connected to the satellite which provides the highest power.

B. Elevation Angle-Based Handover

In this method, the HOs are carried out on the basis of elevation angle, θ, between the user and the satellite. Similar to the previous approach, we consider an offset value before a HO may be triggered. This can be represented by

$$\theta_t > \theta_s + \theta_{off}, \quad (7)$$

where θ_t and θ_s are the elevation angles with reference to target and serving satellites, respectively, and θ_{off} is the offset angle parameter. We assume that the value of θ is perfectly known using the satellite's orbital information and user's location [15]. The initial user association is based on which satellite provides the largest elevation angle.

C. Distance-Based Handover

In the distance-based HO trigger, the same approach is used as the previous methods. There is an offset distance incorporated in the HO triggering mechanism as follows:

$$d_t < d_s - d_{off}, \quad (8)$$

where d_t and d_s are the distances of the users with respect to target and serving satellites, respectively, and d_{off} is the distance offset parameter. The users are initially associated with the satellites that have the smallest distance. This is done by using the location information as described in Section II.

D. Dynamic Threshold

Unlike terrestrial systems, NTNs are dynamic in nature which encourages us to look for dynamic handover thresholds. In this case, we adapt the handover parameter threshold to bias the association towards a satellite moving **towards** a user by selecting a lower offset value (power, angle, or distance) compared to the value chosen for the satellite moving away [16]. This should lead to more stable connections as the user can attach itself more quickly to the satellite coming its way. The decision about coming towards or moving away itself is taken by looking at the progression of the elevation angle between a given satellite and user. If it increases over time, the satellite is assumed to be moving towards the user.

TABLE II
SIMULATION ASSUMPTIONS AND PARAMETERS

Parameter	Values
Environment	Urban
NTN altitude	$\sim$ 550 km
Cell diameter	20 km
EIRP density	S-band: 34 dBW/MHz, Ka-band: 4 dBW/MHz
G_a	S-band: 0 dBi, Ka-band: 39.7 dBi
N_f	S-band: 7 dB, Ka-band: 1.2 dB
T_0	290 K
T_a	S-band: 290 K, Ka-band: 150 K
G/T	S-band: 1.1 dB/K, Ka-band: 13 dB/K
Carrier frequency (f_c)	S-band: 2 GHz, Ka-band: 20 GHz
Bandwidth	S-band: 30 MHz, Ka-band: 400 MHz
Boltzmann constant (k)	-228.6 dBW/K/Hz
Radio link failure (RLF) parameters	$Q_{in} = -6$ dB, $Q_{out} = -8$ dB T310 timer = 1000 ms
TTT	0, 100, 200 (ms)
P_{off}	1, 2, 3 (dB)
θ_{off}	0.5, 1, 2 (°)
d_{off}	1, 5, 10 (km)

IV. MOBILITY KEY PERFORMANCE INDICATORS

Since the system needs to be evaluated for both signaling overhead and link reliability, we look at the number of HOs/UHOs and MToS for the former while RLFs and downlink CNIR are used to evaluate the latter.

A. Number of (Unnecessary) Handovers

Each HO is accompanied by the user terminal spending time searching for a new serving cell and completing the HO process. This involves the transmission of signaling messages, such as handover requests and acknowledgments, which ultimately consumes power. As such, a larger number of HOs not only increases the possibility of disconnection but also decreases the energy efficiency of the system. Additionally, we look at the number of UHOs that occur if a user is handed over from the serving cell to a target cell but stays connected to the latter for $<$ 1s before moving on to a different cell [4].

B. Mean Time-of-Stay

MToS metric gives the average amount of time a user stays connected to a particular satellite before performing a handover to another one. A longer MToS means that the user experiences fewer handovers, which results in fewer disruptions to the user's connection and lower power consumption.

C. Carrier-to-Noise-Plus-Interference Ratio

CNIR measures quality of the radio signal in terms of the power ratio between the desired carrier signal and the combination of noise and interference, where noise is given by

$$N = N_f + 10\log_{10}(T_0 + (T_a - T_0)10^{-0.1N_f}) + k + 10\log_{10} B \quad (9)$$

where N_f, T_0, T_a, k and B refer to the receiver noise figure, reference noise temperature, and receiver antenna temperature, Boltzmann constant, and bandwidth, respectively [17]. Then, downlink CNIR between is calculated using

$$\text{CNIR} = -10\log_{10}(10^{-0.1\text{CNR}} + 10^{-0.1\text{CIR}}), \quad (10)$$

where carrier-to-interference ratio (CIR) is the ratio between the received power from the serving satellite and the sum of the received powers from all other interfering satellites [10], and carrier-to-noise ratio (CNR) is calculated as

$$\text{CNR} = \text{EIRP} - \text{PL}_{\text{tot}} + \text{G/T} - \text{k} - \text{B}, \quad (11)$$

where G/T is the receiver figure of merit.

D. Radio Link Failures

As the name suggests, RLFs indicates the instance where the radio link is degraded to the extent that the link between the network and the user is lost. More specifically, it can be detected if the SINR falls below a certain threshold Q_{out} and fails to improve beyond a higher threshold Q_{in} within a predefined window of time, indicated by the T310 timer [18].

V. Performance Results and Discussion

We considered a simulation area with a diameter of ≈ 20 km, with 100 static[2] users. In order to focus on the radio link itself, we assumed that all HOs that are initiated are successful and any failures that might arise due to network load, etc. are forsaken. For HOs/UHOs/RLFs, the results are averaged over the number of users to give more reliable statistics, while cumulative distribution function (CDF) curves are provided for MToS and CNIR. The simulation duration was taken to be 4 minutes with a measurement recorded every 100 ms. This window size is empirically determined, as we observed that the duration a satellite stayed above 30° elevation angle with respect to the ground users was roughly 4 minutes. The offset values for RSS-related approach were taken from other similar works [2] while those for angle and distance were empirically determined from their observed distributions. For dynamic threshold, the lowest and highest offset values are used for approaching and leaving satellites, respectively. The rest of the simulation parameters are summarized in Table II.

Figure 2 compares the average number of HOs/user for different HO triggers for both S and Ka-band. Results indicate that for optimal association, indicated by P_{max}, the latter requires a larger number of HOs. On the contrary, more HOs are needed for the S-band when P_{off} and TTT are introduced. For both operating frequencies, the best performance is achieved when P_{off} and TTT are set to 3 dB and 200 ms, respectively. Similar performance is obtained for elevation angle and distance-based approaches at both frequencies, with offset values showing limited impact. When dynamic threshold handover is introduced, the number of HOs in power-based triggering for TTT = 0, 100 ms takes an intermediate value (between those of different power offsets). However, for TTT = 200 ms, dynamic power offset slightly increases the number of HOs because a longer waiting time affects the decision. For alternative handover triggers, the dynamic offsets (angle, distance) do not affect the handover performance.

The same trend follows for the UHO rate, as depicted in Fig. 3. However, here the number of UHOs for the alternative methods in both operating frequencies is zero. This is because, unlike the received power-based method, these methods do not suffer from the ping-pong kind of behavior caused by random fluctuations in the observed parameter. Figures 4(a) and 4(b) illustrate the MToS for the different methods for S-band and Ka-band, respectively. As expected, these results are book-ended by P_{max} as the one providing minimum MToS and $P_{off} = 3$ dB with TTT = 200 ms providing the highest MToS for both frequencies. In line with the results of number of HOs/UHOs, the Ka-band shows a higher MToS compared to the S-band. In addition, it is interesting to note that the distance and elevation angle-based methods can provide MToS values of up to 50s and 40s, respectively, which illustrates the relative stability of the connection when these triggers are used. The use of dynamic threshold improves the MToS in the case of TTT $= 0$ ms. Moreover, the angle-based handover has a shorter MToS compared to distance-based one for both frequencies.

Figures 5(a) and 5(b) show the average number of RLFs for the different methods. As expected, this number is the largest for the received power-based method with the highest TTT value which illustrates that the network needs to be much more responsive to avoid RLFs. While P_{max} and different P_{off} values for TTT $= 0, 100$ ms offer low RLFs, this comes with a very high ratio of UHOs for both S-band and Ka-band. The alternative methods, on the other hand, promise low RLFs without causing any UHOs. However, in comparison to the Ka-band, the S-band shows higher RLFs rates not only for conventional triggers but also for alternative handover methods. In the case of dynamic offset handover for the power-based trigger, the number of RLFs for both S-band and Ka-band, is close to that for the case of $P_{off} = 1$ dB which indicates the enhancement of link reliability. Finally, the S-band and Ka-band CDF plots for downlink CNIR are presented in Figs. 6(a) and 6(b), respectively. Starting from the left, we have the performance of different values of P_{off} parameter for the case of TTT $= 200$ ms. This is followed by a cluster of the distance and angle-based approaches for different offset values. However, the difference between them is much smaller compared to the power-based method for both frequency bands. Moreover, P_{max} brings the best case in terms of CNIR distribution. The results indicate that while the case of TTT $= 0$ ms is slightly better than the alternative methods in terms of RLFs per user and the CNIR distributions, this comes at the cost of a significantly large number of

[2]The results in [2] indicate that satellite mobility essentially dwarfs the effect of user mobility due to the sheer difference in their speeds.

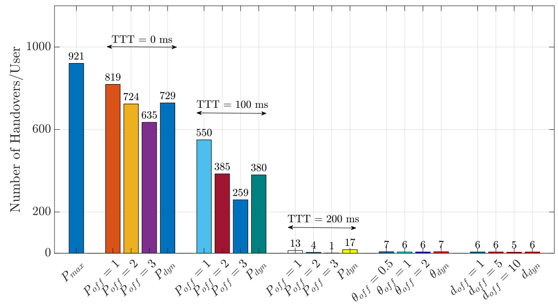

(a)

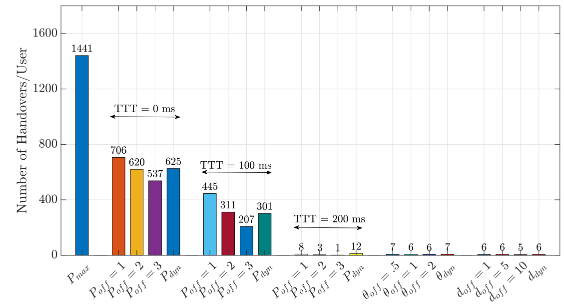

(b)

Fig. 2. Comparison of number of HOs/user for conventional and alternative HO triggering methods for: (a) S-band, (b) Ka-band.

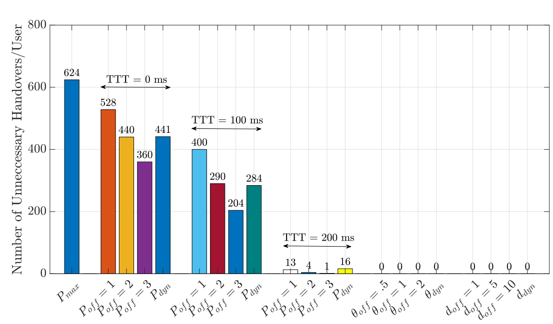

(a)

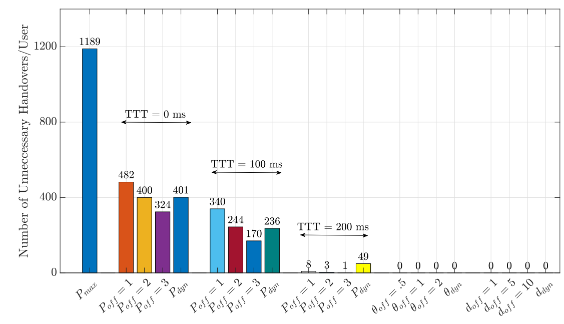

(b)

Fig. 3. Comparison of number of UHOs/user for conventional and alternative HO triggering methods for: (a) S-band, (b) Ka-band.

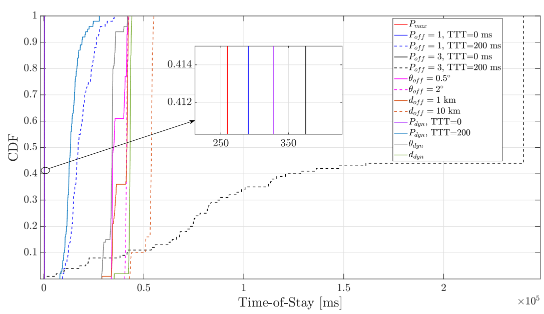

(a)

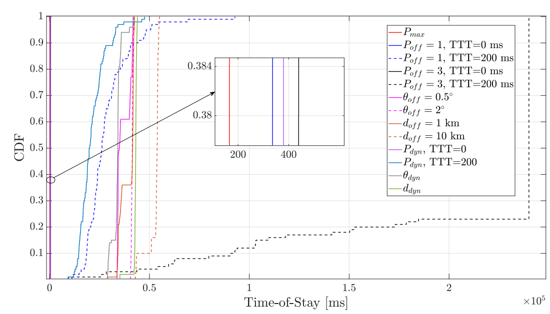

(b)

Fig. 4. MToS comparison between conventional and alternative HO triggering methods for: (a) S-band, (b) Ka-band.

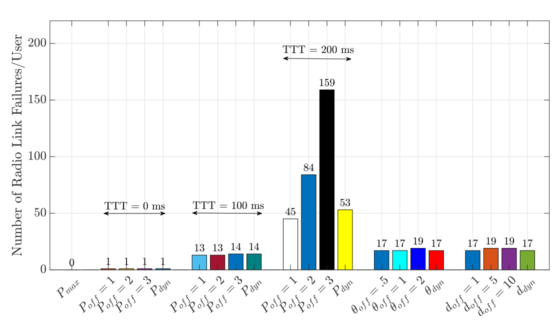

(a)

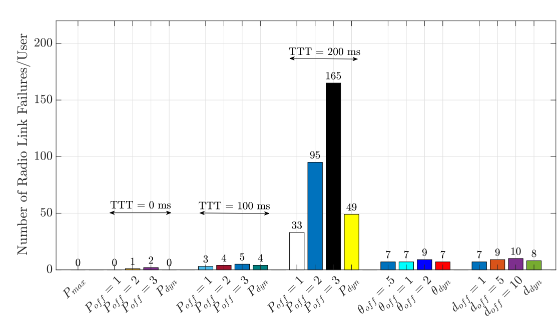

(b)

Fig. 5. RLF comparison between conventional and alternative HO triggering methods for: (a) S-band, (b) Ka-band.

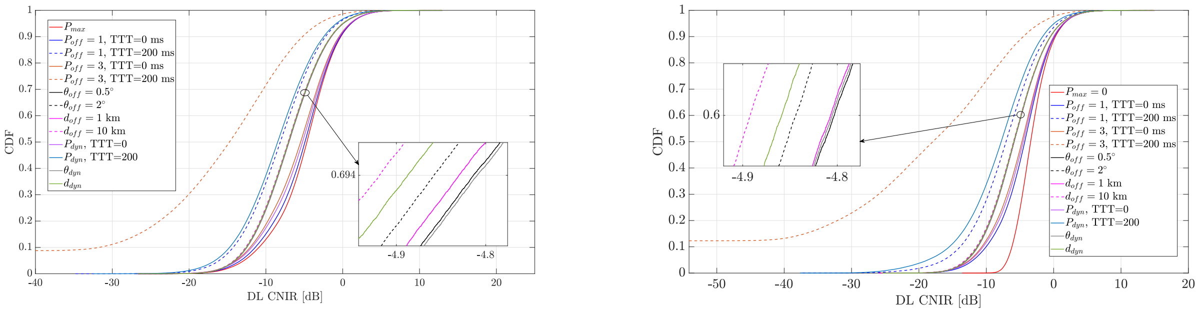

(a) (b)

Fig. 6. CNIR comparison between conventional and alternative HO triggering methods for: (a) S-band, (b) Ka-band.

HOs/UHOs, which indicates the suitability of the elevation angle and distance-based mechanisms in providing a better balance between the overhead and performance of the system. Additionally, the dynamic angle handover performs better than the static case in the S-band, while for the Ka-band the dynamic offset CNIR curve stands between the highest and lowest threshold values.

VI. Conclusion

NTNs have garnered increasing attention over the last few years as the call for global connectivity has picked up pace. While NTNs promises a lot of advantages in this regard, they are also faced with various challenges. Mobility management, particularly for LEOs, is probably the most significant in this regard. Different handover strategies have been discussed for LEOs in S-band scenarios but literature regarding the same in Ka-band is rather scarce. Accordingly, the current work evaluates and compares the performance of not only the conventional received power-based HO triggering, but also alternates such as elevation angle and range-based HO triggers for two different operating frequencies in S and Ka-band. Furthermore, the performance of the above-mentioned triggers based on dynamic control of the threshold is evaluated. This evaluation is carried out in terms of the overhead (UHOs and MToS), as well as communication link quality (CNIR and RLFs). The results, obtained via simulations using real orbital information of satellites indicate the potency of the alternate HO triggers in providing a better balance in terms of overhead and performance compared to the conventional power-based mechanism. Furthermore, based on the results obtained, we can conclude that Ka-band generally outperforms S-band in terms of HO performance. Moreover, the dynamic threshold approach is more supportive of the received power-based HOs. It would be of interest to take into consideration specific user requirements and develop customized HO mechanisms with the objective to maximize the utility of the whole system.

References

[1] E. Juan *et al.*, “5G New Radio Mobility Performance in LEO-based Non-Terrestrial Networks,” in *Globecom Workshops (GC Wkshps)*. IEEE, 2020, pp. 1–6.

[2] Y. I. Demir, M. S. J. Solaija, and H. Arslan, “On the performance of handover mechanisms for non-terrestrial networks,” in *95th Vehicular Technology Conference:(VTC2022-Spring)*. IEEE, 2022, pp. 1–5.

[3] E. Juan *et al.*, “Location-based handover triggering for low-Earth orbit satellite networks,” in *95th Vehicular Technology Conference:(VTC2022-Spring)*. IEEE, 2022, pp. 1–6.

[4] ——, “Performance Evaluation of the 5G NR Conditional Handover in LEO-based Non-Terrestrial Networks,” in *Wireless Communication and Networking Conference (WCNC)*. IEEE, 2022, pp. 2488–2493.

[5] F. Wang *et al.*, “Seamless Handover in LEO Based Non-Terrestrial Networks: Service Continuity and Optimization,” *IEEE Transactions on Communications*, 2022.

[6] E. Juan *et al.*, “Handover Solutions for 5G Low-Earth Orbit Satellite Networks,” *IEEE Access*, vol. 10, pp. 93 309–93 325, 2022.

[7] M. Giordani and M. Zorzi, “Satellite communication at millimeter waves: A key enabler of the 6G era,” in *International Conference on Computing, Networking and Communications (ICNC)*. IEEE, 2020, pp. 383–388.

[8] J. Wang *et al.*, “Deep reinforcement learning-based satellite handover scheme for satellite communications,” in *13th International Conference on Wireless Communications and Signal Processing (WCSP)*. IEEE, 2021, pp. 1–6.

[9] 3rd Generation Partnership Project (3GPP), “Study on New Radio (NR) to support non-terrestrial networks (Release 15),” Technical Report 38.811, ver 15.4.0, Sept. 2020.

[10] ——, “Solutions for NR to support non-terrestrial networks (NTN) (Release 16),” Technical Report 38.821, ver 16.1.0 , May 2021.

[11] CelesTrak, *Starlink TLE Data*, accessed Jan. 20, 2023. [Online]. Available: https://celestrak.org/NORAD/elements/supplemental/sup-gp.php?FILE=starlinkFORMAT=tle

[12] International Telecommunication Union (ITU), “Attenuation by atmospheric gases,” Recommendation ITU-R P.838-3, Aug. 2016.

[13] ——, “Propagation data and prediction methods required for the design of Earth-space telecommunication systems,” Recommendation ITU-R P.618-13, Dec. 2017.

[14] A. Al-Hourani, S. Kandeepan, and S. Lardner, “Optimal LAP altitude for maximum coverage,” *IEEE Wireless Communications Letters*, vol. 3, no. 6, pp. 569–572, 2014.

[15] O. Liberg *et al.*, “Narrowband Internet of Things for Non-Terrestrial Networks,” *IEEE Communications Standards Magazine*, vol. 4, no. 4, pp. 49–55, 2020.

[16] D. A. Blasiak *et al.*, “Method and apparatus for dynamically controlling hand-off thresholds in a satellite cellular communication system,” Aug. 22 2000, US Patent 6,108,538.

[17] A. Guidotti *et al.*, “Non-terrestrial networks: Link budget analysis,” in *International Conference on Communications (ICC)*. IEEE, 2020, pp. 1–7.

[18] 3rd Generation Partnership Project (3GPP), “Evolved Universal Terrestrial Radio Access (E-UTRA); Mobility enhancements in heterogeneous networks (Release 11),” Technical Report 36.839, ver 11.1.0 , Dec. 2012.